2024

Designing an Alginate Hydrogel Wound Dressing for Biofilm Infection Management

Margaret (Maisie) Moses
The University of Vermont

Designing an Alginate Hydrogel Wound Dressing for Biofilm Infection Management

A Thesis Presented by

Margaret (Maisie) Moses

to

The Faculties of the College of Arts and Sciences

of

The University of Vermont

April 2024

Defense Date: April 29, 2024

Thesis Committee:

Dr. Matthias Brewer, Ph.D., Committee Chair

Amber Doiron, Ph.D., Thesis Supervisor

Dr. Jay Silveira, Ph.D., Committee Member

Acknowledgements

Thank you to the Biochemistry Department for Summer Undergraduate Funding and to the National Science Foundation Career Award, through which my research was funded. I would like to thank my supervisor, Dr. Amber Doiron, for exceptional mentorship, unwavering support, and invaluable guidance throughout the project. I would like to thank Omid Sedighi, for his dedication as a mentor and commitment towards my scientific growth and development. Thank you to my committee members, Dr. Doiron, Dr. Brewer, and Dr. Silveira for invaluable insights, feedback, and commitment to the success of this research. Thank you to Dr. Brewer for imparting organic chemistry knowledge and inspiring my interest in medicinal chemistry. Thank you to Dr. Silveira for an enthusiastic teaching style, which ignited my enjoyment for laboratory work and scientific exploration.

Table of Contents

Abbreviations

ATP – adenosine triphosphate

BCA - bicinchoninic acid

$CaCl_2$ – calcium chloride

CoA – coenzyme A

EPS – extracellular polymeric substances

LDH – lactate dehydrogenase

$MgSO_4$ – magnesium sulfate

MOPS - morpholinepropanesulfonic acid

MWCO – molecular weight cut-off

NADH/NAD^+ - nicotinamide adenine dinucleotide

Na-Alg – sodium alginate

PBS – phosphate buffered saline

PDH – pyruvate dehydrogenase

PLGA - Poly(lactic-co-glycolic acid)

SEM – scanning electron microscopy

TPP – thiamine pyrophosphate

UF – ultrafiltered

Abstract

Biofilm infections present a formidable challenge in wound management due to their tolerance to antimicrobial treatments. This study introduces a novel hydrogel wound dressing designed to deplete pyruvate, a key metabolite in biofilm formation and maintenance, from the wound environment. Hydrogel sheets made from the natural polymer alginate crosslinked with

calcium chloride ($CaCl_2$) were synthesized with varied concentrations, with and without the pyruvate-depleting enzyme pyruvate dehydrogenase (PDH). Through analysis of mechanical properties, swelling behavior, morphology, porosity, and enzymatic activity, the study characterizes the hydrogels and demonstrates effective PDH entrapment within the sheets. Results indicate promising potential for biofilm management through pyruvate depletion. Future research will focus on optimizing PDH loading and assessing the dressing's efficacy in biofilm studies.

1. Introduction

1.1 Biofilms

Given their ecological success, biofilms are exceptionally problematic in medical settings. Biofilms are associated with chronic infections in plants and animals, contamination of medical device implants, biofouling water systems, and microbially-affected corrosion.[1] In particular, biofilms thrive in surface wound environments, specifically in burn wounds.[2] Wounds go through three stages in the healing process: inflammation, proliferation, and maturation.[3] Chronic wounds are characterized by persistent infection as the wound is delayed in the inflammatory stage.[4] Biofilms colonize in the inflammation stage, slowing the healing process and contributing to chronic infection. In the United States, about 200,000 people die[5] out of about 6.5 million people who suffer from infections of the dermis, which includes burns, chronic wounds, and surgical site infections.[6, 7] The United States Center for Disease Control states that over 60% of chronic infections are the result of biofilm presence[2] despite improved treatment to reduce wound sepsis.[8, 9] Biofilms can be made up of many strains of bacteria,[1] and some of the most prominent strains known to form biofilms are *Pseudomonas aeruginosa* and *Staphylococcus aureus.*[10-12] Bacteria in biofilms are up to 1000x more tolerant to antimicrobial treatment than planktonic bacteria,[13, 14] making biofilm infections particularly challenging to treat.

Biofilms consist of bacterial communities enclosed in extracellular polymeric substances (EPS).[1] These communities adhere to surfaces, expand in size, and construct a protective matrix, conferring tolerance to conventional treatments.[1] This sets them apart from planktonic, free-floating bacteria. Further, surface-associated growth offers biofilms the ecological advantage of being protected from external environments. While the outside layer of biofilms interacts with the external environment, cells deeper within the community create homeostatic microenvironments.[15] The external cells can interact with hostile factors such as variations in pH or salinity, ultraviolet light, water, and changes in temperature, and they protect the internal cells from antimicrobial agents such as metal ions and antibiotics.[13, 16-19] Biofilms also protect bacterial cells from phagocytosis and immune responses.[20-23] Surface-associated growth allows cells to be in close proximity to each other, which results in enhanced cell to cell communication and horizontal gene transfer.[1] This supports both cell survival and biofilm survival.

The progression of biofilm development involves three fundamental stages. The initial stage encompasses adhesion, aggregation, and the formation of the biofilm structure.[24] The second stage involves growth and maturation, leading to a more intricate and organized structure.[24] Finally, in the third stage, dispersion occurs, with the biofilm releasing planktonic bacteria that adhere to new surfaces, initiating the establishment of new biofilm communities.[24] Dispersed biofilm cells have been reported to be as susceptible to antibiotics and immune responses as planktonic cells.[25, 26] By inducing dispersion to expose cells that can be targeted with antibiotics, biofilm infections can be managed, offering increased recovery rates in chronic wound victims.

1.2 Promising Treatment

The Doiron lab has established that pyruvate depletion prevents biofilm formation, induces dispersion of existing biofilms, and increases susceptibility of dispersed cells to antibiotics and

host immune responses.[12] Researchers in the lab explored exposing biofilms to pyruvate dehydrogenase (PDH) to cause depletion of pyruvate. This treatment has worked to disperse both *Pseudomonas aeruginosa* and *Staphylococcus aureus* biofilms, which are significant pathogens in chronic burn wounds.[12] The Doiron lab compared the efficacy of PDH both alone and in combination with the antibiotic tobramycin on biofilm samples. Results indicate that the PDH + tobramycin treatment significantly reduces biofilm presence compared to free PDH or only tobramycin (Figure 1).

However, translating these findings to a clinical setting presents challenges. PDH is sensitive to storage conditions and loses its activity quickly over time. Further investigations in the Doiron lab involve encapsulating PDH in materials like poly lactic-co-glycolic acid (PLGA) nanoparticles to preserve the activity of PDH.[27] These studies demonstrate how PDH that has been encapsulated in PLGA nanoparticles successfully induces biofilm dispersion. While PLGA nanoparticles were effective, the shape of a wound dressing is desired to maintain wound moisture and promote healing, and alginate is desired to create the hydrogels because it is biocompatible, FDA approved, and able to stabilize enzymes.

1.3 Research Goals

As current treatment options for chronic burn wound infections have proven inefficient, this study aims to investigate encapsulating PDH in alginate hydrogel that meets the physiochemical and mechanical properties of wound dressings as a potential strategy to disrupt biofilms. Alginate is a biocompatible, biodegradable, FDA-approved material that is suitable for wound dressings. It can stabilize PDH and facilitate its use in clinical applications. By targeting pyruvate depletion through PDH, biofilm formation is prevented, and dispersion is induced, rendering the dispersed cells susceptible to antibiotics and the immune system. This study

mechanically, structurally, and physically characterizes the alginate hydrogel sheets through compression testing, swell behavior, and scanning electron microscopy. An optimal formulation is identified for preliminary activity and encapsulation efficiency studies using a β-NADH assay and bicinchonic acid assay.

1.4 Significance of this Study

Determining whether a PDH-alginate hydrogel both prevents and disperses biofilm infections has significant impacts on infectious wound treatment. Pyruvate depleting conditions causes eradication, and this proposed treatment should prevent future biofilm formation. It is important to develop an effective treatment method that circumvents tolerance to current antimicrobial treatment. If the PDH-hydrogel works to both prevent and disperse existing biofilms, then antibiotics have a much higher chance of reaching the dispersed bacterial cells, killing them the first time, without need for a higher dose or multiple rounds of antibiotic treatment. This would decrease infection recovery time, prevent the spread of the infection, and diminish the chance of bacterial resistance. As biofilms are such a significant cause of chronic infections, this proposed wound dressing, in combination with antibiotic treatment, is an extremely relevant and promising infection treatment approach. The implications of this research are vast, offering potential novel strategies for combating chronic infections. Success in using alginate hydrogel as a dispersal agent for biofilms could revolutionize treatment approaches, particularly in chronic wound care.

2. Background

2.1 Current Treatments & Limitations

Current FDA-approved treatment methods for biofilm infections in surface burn wounds include excision, antibiotics, and silver nanoparticles.[8, 9] Excision decreased both the incidence

and mortality rate of burn wound infections through the late 20th century,[8] though excision can result in massive blood loss and scarring, and it does not guarantee eradication of infection. Silver is currently used as a clinical burn wound treatment due to its antimicrobial properties.[28] Silver sulfadiazine is an antibacterial agent that works by releasing sulfadiazine, impairing metabolic functions, when the silver ion binds to bacterial nucleic acids.[29] However, new research has demonstrated that silver cannot distinguish between pathogenic bacteria or healthy immune cells.[28] Also, these therapies typically only work on either gram positive or gram negative bacteria. Biofilms are often made of multiple strains of bacteria, making them especially challenging to treat. Thus, current chronic infection therapies are limited, and there is a need for efficient biofilm treatment.

2.2 Wound Dressings

One way to combat infections is through the wound dressings themselves.[30] Historically, wound dressings served the purpose of protecting the wound from pathogens outside the body, and topical or oral antimicrobials were administered to treat infections.[3] Traditional dressings include gauze, plasters, bandages, and cotton wool, which do not hydrate the wound environment and can be painful during removal.[3, 31] Dressing removal slows the healing cycle because the healing tissue can be removed when stuck to the dry dressing.[3] With surface burn wounds, it is important to maintain a moist wound environment that allows for diffusion of essential molecules. Newer wound dressings have mechanical stability, moisture control, low adherence to the wound, non-toxicity, and biocompatibility.[3, 30] These include biological materials such as allografts, tissue derivatives, and xenografts, or synthetic materials like foams, films, sponges, fibers, and hydrogels.[31] By maintaining wound moisture and having easier removal, the wound dressing is better able to support the healing process.[3]

Hydrogels are a modern type of wound dressing. A hydrogel is a network of polymer chains with the ability to absorb water.[32] Given their ability to swell without breaking down in relatively acidic or basic conditions,[33] they can absorb wound exudate and keep burn wounds hydrated. They also limit trauma to the wound bed because of their mechanical conformability, offering ease of removal.[3] To further support healing, hydrogels can be used for delivery of therapeutics. For instance, antimicrobial agents can be incorporated into hydrogels, and hydrogels can be tuned to release the antimicrobials into the wound environment.[3] Hydrogels offer many features that support the wound healing process and fighting infection.

Alginate is a natural polymer harvested from brown seaweed, which is a material widely used in therapeutic applications as it is biodegradable, easy to make hydrogels from, and biocompatible.[34, 35] Alginate-based treatments already have both FDA approved biomedical and pharmaceutical applications.[36] Hydrogels, particularly those made with alginate, possess promising properties for hosting enzymes and stabilizing them.[27, 37] Because of these properties, alginate treatments can target the delivery of enzymes, cofactors, growth factors, or other substances to a localized region more effectively than other treatments.

2.3 Previous Findings in the Doiron Lab

A promising treatment in the Doiron lab involves modifying the metabolic environment of biofilms. Pyruvate has been shown to promote the formation of biofilms and conversely, in pyruvate-depleting conditions, impair formation.[38] A comprehensive study regarding the underlying mechanism of biofilm formation demonstrated that biofilm formation is correlated with anoxic conditions.[38] Anoxic means without oxygen, as opposed to anaerobic, which means with little oxygen. The Doiron lab studied *P. aeruginosa* in anoxic conditions to see whether biofilms are governed by metabolic pathways or other regulatory mechanisms.[38] *P. aeruginosa* is a model

pathogen for studying biofilms because of its rapid lifecycle and ease of adhering to surfaces, thus allowing biofilms to develop. This study concluded that there are various pathways and mechanisms that contribute to biofilm microcolony formation, but pyruvate is essential for their growth in anoxic conditions.

Biofilms are hypothesized to gain energy from anaerobic respiration because they survive in anoxic conditions.[12, 39, 40] There are two main pathways through which organisms produce energy: aerobic respiration and anaerobic respiration. Glycolysis is the process where organisms convert glucose into energy.[41] A product of glycolysis, pyruvate, is converted by pyruvate dehydrogenase to produce acetyl-CoA, an essential precursor to the citric acid cycle.[41] Under aerobic conditions, the citric acid cycle produces high amounts of ATP from oxidative phosphorylation. However, under anaerobic conditions, the pyruvate fermentation pathway or lactic acid pathway can occur.[42] Under pyruvate fermentation, pyruvate is converted into ethanol via the combined action of pyruvate decarboxylase to produce acetaldehyde followed by alcohol dehydrogenase to create ethanol.[42] Under lactic acid fermentation, pyruvate is converted into lactate via lactate dehydrogenase (LDH).[42] In each of these pathways, the cofactor nicotinamide adenine dinucleotide (NAD^+) is produced, which acts as an electron receptor in ATP-producing metabolic reactions.[41, 42] Since conditions are anaerobic in these pathways, the majority of ATP is produced with NAD^+ driven reactions. NAD^+ must be at high enough concentrations that ATP-generating reactions in glycolysis can continue to provide energy to the organism. Thus, pyruvate is essential to biofilm cells' energy production. Previous work in the Doiron lab studied the impact of both lactate and glucose on biofilm formation and dispersion and found neither to have an impact,[12] emphasizing the importance of pyruvate in biofilm survival.

Additionally, the Doiron lab determined that exogenously produced pyruvate is essential to biofilm structures, specifically in *P. aeruginosa*, *S. aureus*, and *E. coli.*[12, 38] A study conducted by Goodwine et al. supports the essential role of pyruvate in maintaining biofilm integrity.[12] The comparison of biomass, the quantity of organisms in a given volume of biofilm samples, serves as a key metric. The biofilms were exposed to varying amounts of pyruvate dehydrogenase (PDH), an enzyme that metabolizes pyruvate. The biofilm samples treated with PDH exhibit a statistically significant decrease in biomass compared to the control group. The application of crystal violet staining to visualize the biofilms reveals a noticeable outcome: in the PDH-treated samples, the biofilms show signs of dispersion as seen in a clear bacterial sample, indicating disruption of the biofilm structure. The study further tests whether exposing biofilms cofactors CoA and NAD^+ affect biomass – the cofactors were not found to impact biomass.[12] This study shows that pyruvate-depleting conditions via PDH not only prevents biofilm formation but induce dispersion as well.[12] A majority of current treatments for biofilms either target gram positive or gram negative bacteria, but pyruvate depletion via PDH has been found to induce dispersion of both types of bacteria.

This study further explored the combination of exposing *P. aeruginosa* biofilms to PDH plus tobramycin. Tobramycin is an antibiotic commonly used to treat gram negative bacterial infections.[43] The study revealed that a PDH-tobramycin combination therapy significantly reduces biofilms relative to free PDH or free tobramycin treatments, as seen in Figure 1.[12] It demonstrates that inducing biofilm dispersion and then attacking the planktonic bacteria with antibiotics is an effective treatment option. PDH alone is not the therapeutic – combining it with antibiotics bypasses the issue of biofilm tolerance.

One issue with directly treating chronic infections enzymatically is that the treatment is not clinically efficient because enzymes denature in harsh environments. Burn wound temperatures

range from 32°C – 41°C.[44] The pH of a burn wound is 7.6±0.6 in its center and 5.9±0.4 around its borders.[45] The conditions may denature PDH if PDH is exposed directly to wounds. Also, PDH loses activity at temperatures greater than -20°C (Sigma-Aldrich), implying that storage conditions are clinically inefficient. Thus, stabilizing the enzyme in a biocompatible material has been studied.[27]

Han et al.'s research in the Doiron lab highlights the effectiveness of encapsulating PDH in poly(lactic-co-glycolic acid) (PLGA) nanoparticles for biofilm dispersion.[27] The findings suggest that PDH, when effectively encapsulated in the nanoparticles, can disrupt biofilms. This highlights the significance of disrupting pyruvate metabolism as a potential strategy for biofilm dispersal. The approach of encapsulating PDH within PLGA nanoparticles showcases the effectiveness of encapsulating PDH in a material to treat biofilms.

2.4 Hydrogel Design & Research Goals

My study focuses on encapsulating PDH in alginate hydrogels to address the inefficiencies of current treatments for chronic biofilm infections. By removing pyruvate via PDH in the alginate wound dressing, NAD^+ production is greatly decreased, and biofilms are unable to produce enough energy to survive. The unique design of these hydrogels provides a platform for exposure of PDH to biofilm sites. Wound exudate, including pyruvate and cofactors from the wound environment, are expected to absorb into wound dressing. Within the hydrogel pyruvate will be metabolized, inducing biofilm dispersion. Through harnessing pyruvate metabolism via PDH, the approach aims to disrupt the metabolic pathways of biofilms and impair their survival. Once biofilm cells are dispersed, antibiotics and the immune system can effectively target the dispersed cells, enhancing recovery. This design not only leverages the biocompatibility and biodegradability of

alginate but also emphasizes the importance of depleting pyruvate as a critical step towards combating biofilm-associated infections.

My goal is to develop an alginate hydrogel that effectively preserves the activity of PDH while meeting the mechanical and physicochemical properties of commercially available wound dressings and those of a wound environment. The hydrogel is envisioned to absorb pyruvate from the wound environment with exudate from the wound, effectively removing it from the biofilm environment. To ensure the hydrogel's functionality, it should be porous to cofactors and pyruvate but not PDH. Isolated porcine heart PDH complex has a molecular weight of about 8000 kDa and diameter of 45 nm, which includes each of its subunits,[46] guides the design considerations. The hydrogel is not intended to deliver PDH through a release mechanism. Porosity and surface morphology were assessed using Scanning Electron Microscopy (SEM) (JEOL 6060). Current alginate hydrogels typically exhibit pore sizes ranging from 30-450 μm.[47, 48] Elastic moduli, a measure of stiffness, of hydrogel formulations were evaluated using compression testing, assessing the extent of deformation without structural integrity loss (TestResources 240 Universal Test Machine). The hydrogels are designed to be removable while conforming to the wound site, maximizing surface exposure to the wound. Commercial hydrogels demonstrate a swell ratio range from 100% - 1200%,[48-50] indicating their ability to absorb wound exudate without fully dehydrating the wound environment.

2. Materials and Methods

2.1 Materials

Sodium alginate, calcium chloride, PDH from porcine heart, phosphate buffered saline (PBS), thiamine pyrophosphate (TPP), coenzyme A (CoA), magnesium sulfate ($MgSO_4$), pyruvate, β-nicotinamide adenine dinucleotide sodium salt (β-NAD^+), sodium citrate, and 3-N-

(morpholino)propanesulfonic acid (MOPS) were purchased from Sigma-Aldrich (St. Louis Missouri, USA). The pyruvate assay kit was purchased from ScienCell (Carlsbad, California, USA) and the bicinchoninic acid (BCA) protein assay kit from ThermoFisher Scientific (Waltham, Massachusetts, USA).

2.2 Synthesis of Alginate – Sheets

Briefly, sodium alginate was dissolved in ultrafiltered (UF) water to create 1%, 2%, 2.5% and 3% (w/v) solutions. The solutions were poured into 12 mm x 12 mm molds and frozen at -20°C. Ionically crosslinked hydrogel sheets were crosslinked with 0.1 M, 0.2 M, 0.3 M, 0.4 M, 0.5 M, and 1.0 M calcium chloride added dropwise onto the frozen sheets until the sheets were submerged. The sheets crosslinked for 10 minutes, and calcium chloride was added to the bottom of the sheets using gel-loading pipette tips. Crosslinking occurred for 30 minutes in the mold. Sheets were then submerged in calcium chloride solution and rocked for 35 minutes. Sheets of uniform size were produced by carefully removing them from the mold. See Figure 2 for a diagram of this process.

For enzymatic studies, 2084, 2778, and 3473 mU of PDH were mixed into 2% (w/v) sodium alginate solutions to create sheets (n = 3). Sheets without PDH (n = 3) were used as a negative control and free 0.5 mU/µL PDH solutions (n = 5) were used as a positive control to compare pyruvate depleting conditions in the free PDH vs in sheets.

2.3 PDH Buffer Exchange

To ensure that the PDH storage solution did not interfere with downstream applications, PDH was subjected to buffer exchange using Vivaspin® concentration columns with a molecular weight cutoff (MWCO) of 10,000 (Sartorius). The membranes of the columns were pre-rinsed to remove trace amounts of glycerine and sodium azide by addition 500 µl 50 mM MOPS pH 7.4 per

column, 10-minute spin, and decanting of the filtrate. Then, each Vivaspin® column was then disinfected with the addition of 500 µl 70% ethanol, followed by a 10-minute spin, and decanting of the filtrate. Residual ethanol was removed by washing each column 3 times with 500 µl 50 mM MOPS, followed by a 10-minute spin, and decanting of the filtrate.

Briefly, PDH was diluted to 0.5-2 mU/µl in 50 mM MOPS pH 7.4 and washed using Vivaspin® 500 µl 10,000 MWCO concentration columns. All spins were carried out at 4°C in a 45° fixed angle rotor using Centrifuge 5424R (Eppendorf) at 15,000 x g. To swap PDH from the storage solution to 50 mM MOPS pH 7.4, 500 µl of 0.5-2 mU/µl, PDH was added to each column, columns were spun for 40 minutes, and filtrate was decanted. The columns were then washed 3 times with 500 µl 50 mM MOPS pH 7.4, a 40-minute spin, and filtrate decanting. Following the third wash, the concentrate containing the PDH was collected using gel-loading pipette tips. The concentrate was then brought back up to its initial 500 µl volume in 50 mM MOPS pH 7.4. The buffer exchanged enzyme was aliquoted to 50 µl and stored at -20°C to be used in downstream applications.

2.4 Enzymatic Activity & Encapsulation Efficiency

PDH activity was calculated by the conversion of ß-NAD^+ to ß-NADH over 60 minutes (Δ340nm/60 min) using an extinction coefficient of 6.22 $mol^{-1} \times cm^{-1}$.[27] The protocol as described in Han et al. was followed.[27] Reactions were carried out at room temperature in 1 mL. The concentrations of PDH cofactors were as follows: 2 mM NAD^+, 2 mM CoA, 20 µM TPP, 50 µM $MgSO_4$, and 10 mM pyruvate.[27] Volumes of 100 µL of each reaction were loaded into a 96-well plate, and absorbance at 340 nm was recorded at t = 0, 30, 60, 90, 1080, and 2520 minutes at 25°C using a microplate reader (Molecular Devices SpectraMax i3x). Positive controls were free PDH solutions and negative controls were sheets with 0 mU of PDH.

To determine encapsulation efficiency, hydrogels were dissolved in 16.7 mM sodium citrate. Micro BCA Working Reagent (WR) was prepared as follows: Reagent MA (alkaline tartrate-carbonate buffer), Reagent MB (BCA solution), and Reagent MC (copper sulfate solution) were mixed according to a ratio of 25:24:1. Microplate wells were filled with 150 µL of each standard or unknown sample replicate. Subsequently, 150 µL of Micro BCA Working Reagent (WR) was added to each well. The plate was then thoroughly mixed on a plate shaker for 30 seconds and incubated at 37°C for 2 hours. Following incubation, absorbance at 562 nm was measured using a plate reader. The average absorbance reading of the blank standard replicates was subtracted from the absorbance reading of each individual standard and unknown sample replicate. A standard curve was prepared by plotting the average blank-corrected absorbance reading for each Bovine Serum Albumin (BSA) standard against its known concentration in µg/mL. Encapsulation efficiency was calculated as:

$$Encapsulation\ efficiency = \frac{amount\ of\ PDH\ encapsulated\ in\ sheets\ (mg)}{amount\ of\ PDH\ used\ (mg)} * 100$$

2.5 Characterization of Hydrogels

2.5.1 Uniaxial Unconfined Compression Testing

The compressive elastic moduli of all hydrogel formulations (Table 1) were determined. Compression tests were conducted using an electromechanical universal testing machine (Test Resources, 200 series, Shakopee, MN, USA) 5 kN load cell (Test Resources, model no. SM-5000N-294, Shakopee, MN, USA) and 56-mm diameter compression platens (Test Resources, model no. G23). Hydrogel sheets (12 mm x 12 mm) (n = 4) from each group were made and hydrated in UF water. Samples were placed on the compression plates and the machine was lowered until the upper compression platen lay flat on the top of the hydrogel sheet. The gap height was noted as the initial gauge length for displacement measurements. The sheets were

subject to uniaxial compressive loads at 5 mm/min. Elastic stress and strain values were plotted. The elastic modulus for each sample was calculated as the slope of the linear region in 10% compressive strain within the linear elastic region of the stress-strain plots.[51]

2.5.2 Swell Testing and Hydrolytic Degradation

The hydrogels were freeze-dried, and initial dry weights (W_i) were measured. The dried samples were immersed in 5 mL of 1X phosphate buffered saline (PBS) pH 7.4 or UF water and incubated at 37°C. At days 1, 7, 14, and 21, samples were removed, and the wet weights (W_w) were measured. For each time point, three gels per composition were measured. The samples were freeze-dried, and dry weights (W_d) were recorded for each time point. Swell ratio was calculated by:

$$\textit{Equilibrium swell ratio (\%)} = \frac{(swollen\ weight - initial\ dry\ weight)}{initial\ dry\ weight} * 100$$

Hydrolytic degradation was calculated by[49]:

$$\textit{Weight loss (\%)} = \frac{(initial\ weight - dry\ weight)}{initial\ weight} * 100$$

2.5.3 Scanning Electron Microscopy

Immediately after crosslinking, hydrogel samples were flash-frozen in liquid nitrogen to maintain the internal structure of the scaffold. The samples were lyophilized once frozen, cut with a razor blade, and sputter-coated with gold prior to imaging. Scanning electron micrographs (Zeiss Sigma 300 VP Field-Emission SEM, Oberkochen, Germany) were used to qualitatively characterize the internal structure of the crosslinked scaffolds and confirm an interconnected porous network.

2.6 Statistical Analysis

Results were expressed as averages ± standard error. All averages were taken with n = 3 unless otherwise noted. A Two-Way Analysis of Variance (ANOVA) was performed to determine

the statistical significance between groups and Tukey's Multiple Comparison post hoc tests were used to compare means. A 5% significance level was used. The effect of independent variables such as $CaCl_2$ concentration, Na-Alg concentration, and amount of PDH on outcomes such as elastic modulus, swell ratio, hydrolytic degradation, and PDH activity, and PDH encapsulation efficiency were analyzed using GraphPad Prism v 10.1.1 (GraphPad Software) and JMP Pro 15 v 15.2.1 (JMP® Software).

3. Results

3.1 Compression Testing

The hydrogel sheets were made via ionic crosslinking of various formulations of sodium alginate and calcium chloride concentrations (Table 1), which is a well-established process as reported in literature.[52, 53] Uniaxial compression testing was done to measure the elastic modulus of samples to determine whether these sheets meet the elastic modulus threshold of commercially available hydrogel wound dressings. Literature reports that ionically crosslinked alginate hydrogels have elastic moduli in the range of 30-550 kPa.[48, 49, 54] Compression tests were run on n = 4 samples and elastic modulus, which is a measure of stiffness, was calculated by interpolating the 10% linear region from the stress strain plot. Stress is force per area and strain represents a displacement from the starting point. The slope of the linear region represents elastic modulus.

As seen in Figure 3, the elastic modulus appears to either decrease or stay consistent as sodium alginate concentration increases as calcium chloride concentration is constant. The average elastic modulus is around 50 kPa for many of the samples, with the 1% (w/v) sodium alginate samples having higher elastic moduli.

A Two-Way ANOVA revealed that there was not significant interaction between both sodium alginate and $CaCl_2$ concentrations, but it revealed that sodium alginate concentration is

statistically significant at $\alpha = 0.05$ ($p = 0.0282$) and accounts for 9.910% of the total variation in elastic modulus (Calculated on GraphPad Prism v 10.2.1).

3.2 Equilibrium Swell State & Hydrolytic Degradation

Moving forward with reliable materials for equilibrium water content and hydrolytic degradation tests, tests were conducted at body temperature (37°C) to determine whether the degree of crosslinker or alginate concentration affected the weight loss or swelling behavior and whether there was a trend in the results. Hydrogel compositions from a subsection of Table 1, highlighted in yellow, were chosen for this study because they most consistently met commercially available standards defined by the elastic modulus values from compression testing and qualitative standards such as appeared homogeneity.

The first study was completed over the course of 21 days in PBS pH 7.4 to simulate biological conditions. As seen in Figure 4c, there is an apparent trend: with increasing sodium alginate concentration, swell ratio decreases. Similarly, with a higher degree of crosslinking within each sodium alginate concentration group, there is a lower swell ratio. The highest swell ratio in PBS was found to be 3149.42% in a 2.5% (w/v) Na-Alg & 0.3 M $CaCl_2$ formulation at Day 14 while the lowest was 1052.31% in a 3% (w/v) Na-Alg & 0.5 M $CaCl_2$ formulation at Day 1. There was not a significant difference in swell ratio from day to day.

The hydrolytic degradation studies in PBS revealed that the 0.4 M $CaCl_2$ hydrogel samples had the greatest percent weight loss, while the 0.3 M $CaCl_2$ samples had the least percent loss (Figure 4a). Some of the values were negative, which indicates that those samples gained mass through the hydration process. A Two-Way ANOVA revealed that there is a significant association between calcium chloride concentration and percent weight loss ($p = 0.0003$).

Given that there appeared to be observed physical degradation and larger measured masses after increased amounts of time, this study was replicated using water to determine whether salt deposits from the PBS caused the increases in mass. Performing the same study in water, at Day 1, most of the samples had a 20-40 percent weight loss, and the percent weight loss decreased from time point to time point by over 20% for many of the samples (Figure 4b). There is a significant association between calcium chloride and percent weight loss ($p = 0.0048$).

For the swell ratio measurements, there also was an apparent negative trend between swell ratio and sodium alginate concentration, as seen in Figure 4d. The highest swell ratio was 1945.95% in 2% (w/v) Na-Alg & 0.3 M $CaCl_2$ and the lowest was in the 3% (w/v) Na-Alg & 0.5 M $CaCl_2$ composition at 1094.02%. A Two-Way ANOVA revealed that calcium chloride concentration is significant for the overall equilibrium swell model ($p = 0.0074$), but Tukey post hoc comparisons did not reveal any significant differences between each calcium chloride formulated sample and swell ratio within each time point.

In comparing the swell ratio results in water and PBS, overall, the swelling capacity was greater in PBS than in water. For both, there is a trend where increasing sodium alginate concentration decreases swell ratio. This suggests that the hydrogels can be tailored to the wound site's physiochemical properties to best support infection management.

After determining 2% sodium alginate and 0.3 M $CaCl_2$ to be an optimal formulation, swell ratio studies were done to determine the impact of pH on swell behavior. As seen in Figure 5, there appears to be a positive trend: with increase in pH, swell ratio increases. A Two-Way ANOVA revealed that pH is statistically significant (p-value < 0.0001). Tukey post hoc comparisons revealed that at 6 hours, pH 5.5 and pH 7.5 are statistically significant ($p = 0.0013$), 24 hours, pH 5.5 and pH 7.5 are statistically significant ($p = 0.0021$), 36 hours, pH 5.5 and pH 7.5 are statistically

significant ($p = 0.0013$), and 48 hours, pH 5.5 and pH 7.5 are statistically significant ($p = 0.0368$). This demonstrates that pH does have an impact on swelling capacity of alginate hydrogels.

3.3 Scanning Electron Microscopy

The morphology and porosity of samples were characterized with scanning electron microscopy (SEM). SEM images confirmed the presence of an interconnected porous network. In the 2% (w/v) Na-Alg & 0.3 M $CaCl_2$ sample, the external surface has pores with an average size of 45.409 ± 28.906 μm ($n = 20$) while the cross-sectional surface, after being cut with a razorblade, has average pore sizes of 88.375 ± 39.329 μm ($n = 29$). In the 2% (w/v) Na-Alg & 0.5 M $CaCl_2$ samples, the average pore size of the external surface is 40.607 ± 32.555 μm ($n = 14$) and the cross-sectional surface is 60.969 ± 24.455 μm ($n = 10$). In the 3% (w/v) Na-Alg & 0.5 M $CaCl_2$ samples, average pore size in the external surface is 25.726 ± 16.969 μm ($n = 3$) and 43.853 ± 23.954 μm ($n = 11$) in the cross-sectional surface. This reveals that higher degree of crosslinker, and sodium alginate concentration creates a tighter network with smaller pores.

Without accounting for whether the surface is an external surface or cross-sectional surface, a Two-Way ANOVA revealed that calcium chloride concentration is significant for the model ($p = 0.0163$). Tukey post hoc tests revealed that the 2% Na-Alg & 0.3 M $CaCl_2$ and 3% Na-Alg & 0.5 M $CaCl_2$ pore sizes are significantly different than each other ($p = 0.0294$), indicating that higher degree of crosslinker and alginate concentration results in lower pore sizes.

After running a One-Way ANOVA test comparing the pore sizes for the external surface, the pore sizes between each formulation for the external surface were not significantly different than each other ($p = 0.7645$). A One-Way ANOVA was used to compare the pore sizes of each formulation of the cross-sectional surfaces, and the means were found to be significantly different ($p = 0.0014$). A Tukey post hoc test revealed that the 2% (w/v) Na-Alg & 0.3 M $CaCl_2$ average

pore size is significantly different than 3% (w/v) Na-Alg & 0.5 M $CaCl_2$ average pore size ($p = 0.0016$) of the cross-sectional surface. Again, this demonstrates that increasing crosslinker and alginate concentration results in smaller pores in the hydrogel scaffold.

3.4 Pyruvate Depletion and Enzymatic Activity

The BCA assay quantified PDH encapsulation in the hydrogel sheets. It showed a concentration dependent trend with average entrapment efficiency at 8.88%. Comparatively, PGLA nanoparticles had an encapsulation efficiency of 9%.[27]

The pyruvate assay quantified average activity of the PDH before encapsulation at 9.07±3.2 mU/mL, which is within the 5-10mU/mL range necessary to induce biofilm dispersion. Increasing PDH from 2084 to 3473 mU in the hydrogel sheets resulted in an activity increase from 0.7 to 2.02mU/mL. This confirms the ability of hydrogel sheets to cause pyruvate depleting conditions that result in induction of biofilm dispersion.

4. Discussion and Future Direction

4.1 Mechanical, Physical, and Structural Properties

Alginate is made up of 1-4 linked β-D-mannuronic and α-L guluronic acid residues.[55] The linear polysaccharide structures are composed of monomer residues linked in varying compositions,[56] creating an egg-crate like structure (Figure 6). The divalent calcium ions can penetrate into the openings in the polymer crate structure and form ionic bonds with the carboxyl groups in the alginate, creating a uniformly crosslinked structure.[53] Increasing the concentration of calcium chloride crosslinker improves mechanical properties like elastic modulus.[57] Mechanical properties can further be tailored through polymer concentration.[54]

Preliminary studies in the Doiron lab used a sodium alginate concentration of 2% (w/v) for creating hydrogel samples in bead form. Calcium chloride concentrations of 0.1 M, 0.2 M, 0.3 M,

0.4 M and 0.5 M were used in those studies. Also, 1% and 3% sodium alginate concentrations and 1.0 M $CaCl_2$ were used in other hydrogel sheet studies.[48] The hydrogel concentration matrix (Table 1) was created based on these parameters. The maximum sodium alginate concentration at 3% (w/v) was chosen as the largest because the high viscosity resulted in difficulty measuring and mixing the solution. Samples made with this concentration tended not to fully crosslink, which likely affected the compression testing results. A higher concentration likely would have been too viscous to continue with experimentation.

Hydrogel wound dressings must be stiff enough to conform to the wound site yet flexible enough to allow for ease of removal. By characterizing mechanical properties such as elastic modulus as a measure of stiffness, clinical applicability can better be predicted. We expected elastic modulus to increase as calcium chloride concentration increased because increased crosslinker should stiffen the gel.[54, 57] Similarly, we expected increased sodium alginate concentration to increase elastic modulus because there is more polymer available for the crosslinker to interact with.[54] Literature has shown these trends to be true for similarly formulated hydrogel materials, though sodium alginate concentration appears to impact elastic modulus more than calcium chloride concentration does.[54, 57]

Although the statistical analysis revealed that sodium alginate concentration is significantly associated with elastic modulus in the overall model, within each calcium chloride concentration, there was not a significant association or trend of increased elastic modulus with increase in sodium alginate concentration. The discrepancy between the results of this study and trends recorded in literature could be due to a lack of sensitivity of the machinery used for testing. We used a 5 kN load cell and 56 mm diameter platens for compression testing. Given that the sheets were much smaller, about 12 mm x 12 mm and about 3 mm thick, these platens may have been

too large and the load cell too insensitive for accurate compression testing, resulting in inaccurate elastic moduli. However, studies that used the same equipment and set up for the same purpose obtained published results.[48] This suggests that the results were not attributable to user error, but rather an insensitivity of machinery.

Overall, the compression testing results support that increasing sodium alginate concentration is significantly associated with elastic modulus. The results support that the mechanical properties of sodium alginate hydrogels can in fact be tailored to meet commercial needs, but further testing needs to be done to determine the optimal sodium alginate concentration and calcium chloride concentration to achieve optimal stiffness, characterized through elastic modulus. Even though the trend was different than expected, the hydrogels met the standards being tested for.

The 1% (w/v) Na-Alg sheets had very small physical structures and were heterogenous. Ideally, the sheets should be homogenous structures when they form to ensure that the enzyme, PDH, is distributed uniformly across the sheet for maximum exposure to the wound environment. Sheets formed using 0.1 M and 0.2 M $CaCl_2$ did not fully crosslink across each of the four batches, so those calcium chloride concentrations were deemed unsuitable for further study. The low degree of crosslinker may have taken too long for crosslinking in the protocol we used; the gel did not form quickly enough to maintain the shape of a sheet. Again, complete crosslinking is essential in synthesis of the sheets to ensure homogeneity. The 0.3 M, 0.4 M, and 0.5 M $CaCl_2$ concentrations produced elastic modulus values most consistently found in commercially available range and met qualitative homogeneity and structural standards, so these concentrations were identified as appropriate for further testing.

After determining an optimal formulation range based on the elastic modulus values and qualitative observation, the hydrogels were physically characterized by studying swell behavior and hydrolytic degradation. Swell ratio is a measure of a material's ability to absorb water and in a clinical application, wound exudate. Hydrolytic degradation is a measure of the breakdown of the polymer network, measured in percent weight loss. This is useful in predicting the potential duration of a wound dressing application. We want the wound dressing to maintain wound moisture yet absorb cofactors essential to pyruvate depletion.

The study was first completed in phosphate buffered saline (PBS) at pH 7.4, which is the biologically relevant pH. As seen in Figure 5a, the percent weight loss in PBS was negative, indicating that the hydrogels gained mass. I repeated the study in water to determine whether it was salt from the PBS that caused the gain in mass. In both solvents, a lower degree of crosslinking and less compact alginate network had a higher degree of degradation in alginate hydrogels, which is a trend supported in literature.[58, 59] Similarly, a denser network of hydrophilic groups with an increased alginate concentration would repel water molecules, resulting in a lower degradation rate. The increased crosslinker concentration also would decrease degradation rate because there would be fewer open polar sites for the water molecules to penetrate and interact with, as the sites are more likely to be occupied by ionically bonded calcium ions from the crosslinking solution.

Between the two models of PBS and water, there was not a significant difference in the degradation results to suggest that there is a difference between PBS and water on hydrolytic degradation. The observed difference in swell results and degradation results may be due to the buffering capacity of PBS, solubility of the hydrogels in each solvent, or hydrogen bonding. Since PBS contains ions, the ionic strength of the solution may be affected, and changes in ionic strength may influence the rate of degradation reactions. UF water is a neutral solution without those ions.

However, in a theoretical model predicting swelling kinetics, no distinction is made between using PBS or water as a solvent because the ionic strength (~2.3 mmol/L) of PBS is negligible and its mass density is nearly the same as water.[60] The literature supports that there should not be a significant difference in using PBS or water. To further explain the difference in results, the hydrogels may have different solubilities in water relative to PBS. Since degradation typically occurs at the surface of a material, its solubility can affect the rate of degradation. Also, water molecules can form hydrogen bonds with polar functional groups, affecting accessibility of water molecules to reactive sites, influencing the rate of hydrolysis. Although the functional groups on the alginate polymer are hydrophilic and thus attract water molecules, the overall structure of the polymer backbone may limit water penetration or interaction, resulting in lower degradation rates.

It was expected that there would be a trend found between both calcium chloride concentration and sodium alginate concentration with swell ratio in both water and PBS. Each concentration variable impacts the swell ratio separately. There is not a statistically significant interaction ($p = 0.7203$) between sodium alginate and crosslinker concentrations to impact swell ratio ($n = 3$). In other words, a higher cross-linkage and tighter polymer network results in lower swelling capacity. Lower degree of crosslinking and less alginate has been shown to have greater swelling capabilities due to water being able to diffuse into the hydrogel easier.[58, 59] Further, the backbone of the alginate polymers repels water because of its hydrophilic groups. With more hydrophilic groups to repel water, water interacts less. Comparatively, commercial hydrogels have a swell ratio from 100-1200%. The synthesized hydrogels consistently meet if not exceed this standard, demonstrating the ability of these hydrogels to theoretically absorb wound exudate while maintaining wound moisture.

A swell study was then done to determine whether pH has an influence on swell behavior because the pH of a burn wound is 7.6 ± 0.6 in its center and 5.9 ± 0.4 around its borders.[45] The statistical significance between pH 5.5 and pH 7.5 at nearly each time point, as seen in Figure 5, suggests that the wound dressing may have imbalanced swelling capabilities across the wound bed since the pH is different across the wound surface. The carboxylic acid functional groups in the alginate polymer can become protonated or deprotonated, depending on the pH, which can affect the interaction between the alginate chains and calcium ions, ultimately impacting swell ratio and degradation. The pH can also influence accessibility of water molecules to the hydrogel, impacting swelling kinetics and equilibrium water content. This study demonstrates that even after crosslinking occurs, pH has an influence on swelling behavior and degradation, and it is a variable that should be taken into consideration in future studies.

Through studying the swelling behavior of the hydrogels, it is known that molecules such as water can diffuse into the sheets. For application of these hydrogels as wound dressings, swelling is important so that the hydrogel can uptake pyruvate and other cofactors, so they interact with the entrapped PDH. Both the external and internal pores must be large enough for those molecules to pass through yet small enough for PDH to stay entrapped.

As seen through the SEM images in Figure 7 and the results in Table 2, the overall pore size both on the external surface and internal network of the hydrogels are within commercially available alginate hydrogel pore size range of 30-450 μm.[47, 48] The standard deviation is so large for each of the samples because of the elongated shape of some of the pores. Some measurements represent the width while others represent the length of the elongated structures, but other pores were circular. This made it difficult to accurately measure average pore size since the shape of the

pores was inconsistent. However, the differing pore structure likely contributes to the encapsulation of PDH and prevents PDH from escaping the network.

Qualitatively, the pores of 2% (w/v) Na-Alg & 0.3 M $CaCl_2$ sheets were elongated oval-shaped structures, as seen in Figure 7a, on the external surface. The top surfaces generally look much smoother than the inside surface, which makes sense because the inside morphology should have been preserved with the sharp razorblade cut while the outside surfaces may have been affected through the freeze-drying process. It suggests that there will be less electrostatic interactions at the surface of the hydrogels such that small molecules, including water, will be able to be absorbed into the material relatively easily. This is important for absorption of cofactors and pyruvate, so they interact with PDH. The pores also appear twisted, confirming that the large PDH molecules, about 45 nm in size, will likely stay inside the sheets.

The porosity promotes wound healing by allowing for the diffusion and exchange of essential molecules from the wound and the external environment. Essential molecules include oxygen, carbon dioxide, water, and glucose. Oxygen/carbon dioxide exchange is required in the healing process because oxygen is an important part in energy production that powers cell proliferation, collagen synthesis, and angiogenesis.[61] Carbon dioxide plays a role in regulating activity of macrophages, which clear debris and pathogens during early stages of wound healing, and vasodilation, which facilitates delivery of oxygen and other nutrients by improving blood flow to the wound site.[62] In pH levels measured in burn wounds, pyruvate exists in its deprotonated state because of its low pKa of 2.5.[45, 63] Clinically, pyruvic acid is able to diffuse through this scaffold as it is a small molecule at 10 atoms.[45] Other cofactors involved in the catalysis of pyruvate to acetyl-CoA by PDH include TPP, NAD^+/NADH, CoA, and $MgSO_4$. These molecules are also small enough to diffuse into the hydrogel and interact with PDH.

The tortuous internal structure of the hydrogels, as visualized in Figure 7, demonstrates that PDH should be entrapped in the structure through the crosslinking process. PDH is a large, 3-subunit enzyme at about $3.8x10^3$ kDa with a diameter ranging from 25-45 nm, depending on the source of PDH.[46, 64, 65] Comparatively, the molecular weight of pyruvate is about 87 Da.[27] Given the tortuosity of the hydrogel scaffold, it is easier for pyruvate and the other various cofactors to diffuse into a hydrogel rather than design a material that PDH can diffuse out of. The porosity supports the hypothesis that PDH can be entrapped in an alginate hydrogel, and cofactors will be able to diffuse into it. This study confirms that we can make tunable ionically crosslinked alginate hydrogels because the Two-Way ANOVA analysis revealed that calcium chloride concentration is significantly associated with pore size ($p = 0.0163$).

4.2 Enzymatic Function

A preliminary enzymatic study confirms that the mechanically, physically, and structurally characterized the alginate hydrogels do in fact induce pyruvate depleting conditions. The Doiron lab already established that encapsulating PDH in PLGA nanoparticles induces depletion of pyruvate and dispersion of biofilms, but I wanted to see whether it did in alginate hydrogel sheet form.

PDH activity was quantified through the conversion of β-NAD^+ to β-NADH over 60 minutes by measuring the change in absorbance at 340nm/60 minutes, which is proportional to the pyruvate concentration.[66] β-NAD^+ has a specific absorbance at 340nm, which allows the reaction to be quantified. Free PDH with 0.33 mU activity was tested because it represents the lower bound

of PDH activity (0.5 mU/μL) needed to induce pyruvate depleting conditions.[12, 27] This range was determined experimentally.

It was initially expected that with increasing enzyme to the reaction, the loading of PDH would increase and then plateau, which would indicate PDH saturation in the sheets.[27] Similarly, a higher level of activity was expected with an increased amount of PDH.[27] The sheets without PDH did not display activity, which was expected as a control. The free PDH samples had an average activity of 9.07 mU/mL, which is in the pyruvate depleting range. The results in Table 3 indicate that PDH activity increases in a concentration dependent manner. As the amount of PDH loaded into the sample increases, activity increases at each time point. For example, activity increases from 0.7 to 2.02 mU/mL at 90 minutes. Activity also appears to increase with time, but it decreases after 2 days. These results are promising because it shows that activity is retained over time when PDH is encapsulated in alginate hydrogel sheets, which is one of overarching goals of the project.

The 8.88% encapsulation efficiency in the sheets is similar to the efficiency seen with PLGA nanoparticles (9%).[27] This demonstrates that PDH can successfully be encapsulated into hydrogel sheets with similar efficiency to a nanoparticle form. However, this is a relatively low percentage, and further research is needed to determine the optimal PDH concentration to add to the hydrogels such that optimal encapsulation efficiency is reached.

4.3 Limitations

Acknowledging that this method of treatment has limitations such as storage stability, ideal duration of application, and decreased PDH activity in suboptimal conditions, this wound dressing is one of many ways to help treat chronic surface wounds. PDH has an optimal function from pH 7.3-7.7.[67] Burn wounds have a pH range from 5.9 – 7.6. The wound dressing should protect the

activity of PDH due to its design, but this is something that future research can address. PDH has an optimal storage temperature of -20°C (Sigma-Aldrich), which has implications for transportation difficulties should this wound dressing become commercialized. However, encapsulating PDH in an alginate hydrogel should improve its storage capabilities. Further study can investigate optimal storage conditions and potentially tailor the wound dressing to have a larger range of storage conditions including pH and temperature. Another limitation to my study is that the mechanical, physical, and structural characterization studies were done without PDH encapsulated in the hydrogels. PDH is a large complex, and it may have an influence on stiffness, swell behavior, and pore size once encapsulated. Future investigation can repeat my experiments with PDH. Despite the limitations to a clinically complex issue, the wound dressing treatment is one possible way to manage biofilm infection and improve recovery rate in chronic surface burn wounds.

5. Conclusion and Further Direction

The findings from this study hold significant implications for the treatment of chronic burn wound infections. The investigation into encapsulating PDH in alginate hydrogel aimed to address the inefficiency of current treatment options by disrupting biofilms. A hydrogel was created that mimicked the mechanical and physicochemical properties of burn wounds, envisioned as a vehicle for absorbing pyruvate from the wound environment and removing it from the biofilm matrix.

Overall, these findings underscore the potential of PDH-hydrogel sheets in biofilm dispersion strategies, offering control over pore size, elastic modulus, swell ratio, and degradation behavior. The optimal formulation thus far - identified as 2% (w/v) Na-Alg & 0.3 M $CaCl_2$ - exhibited promising characteristics, including suitable pore morphology and controlled swell behavior. Importantly, the hydrogel's porous structure suggests easy passage of cofactors and

pyruvate while retaining PDH molecules, aligning with the design objectives. Additionally, the mechanical properties of the hydrogel, including its elastic modulus and swell ratio, met the desired criteria for conforming to wound sites and absorbing exudate without dehydrating the wound environment excessively.

Our results demonstrate successful encapsulation of PDH in alginate hydrogel sheets, with quantifiable entrapment efficiency and the ability to induce pyruvate-depleting conditions. By creating pyruvate-depleting conditions, the hydrogel meets the goal of encapsulating PDH to trigger these conditions. Further research will optimize the PDH loading and encapsulation efficiency before in vitro and in vivo studies with biofilms. Given that the PDH-hydrogel can deplete pyruvate, optimizing the PDH concentration is the next step in optimizing this therapy.

Goodwine et al. demonstrated that co-administration of 100mU or 200mU of PDH with tobramycin, an antibiotic, on porcine burn wounds significantly increased the efficacy of tobramycin.[12] Additional future research can determine appropriate dosing of antibiotics in addition to the PDH-wound dressing to evaluate efficacy of the combined treatment.

Ultimately, this research presents a promising step towards revolutionizing infection treatment approaches, particularly in chronic wound care. The implications of using PDH-alginate hydrogels as a dispersal agent for biofilms extend far beyond burn wound infections, offering potential novel strategies for combating various chronic infections and improving patient outcomes.

Tables & Figures

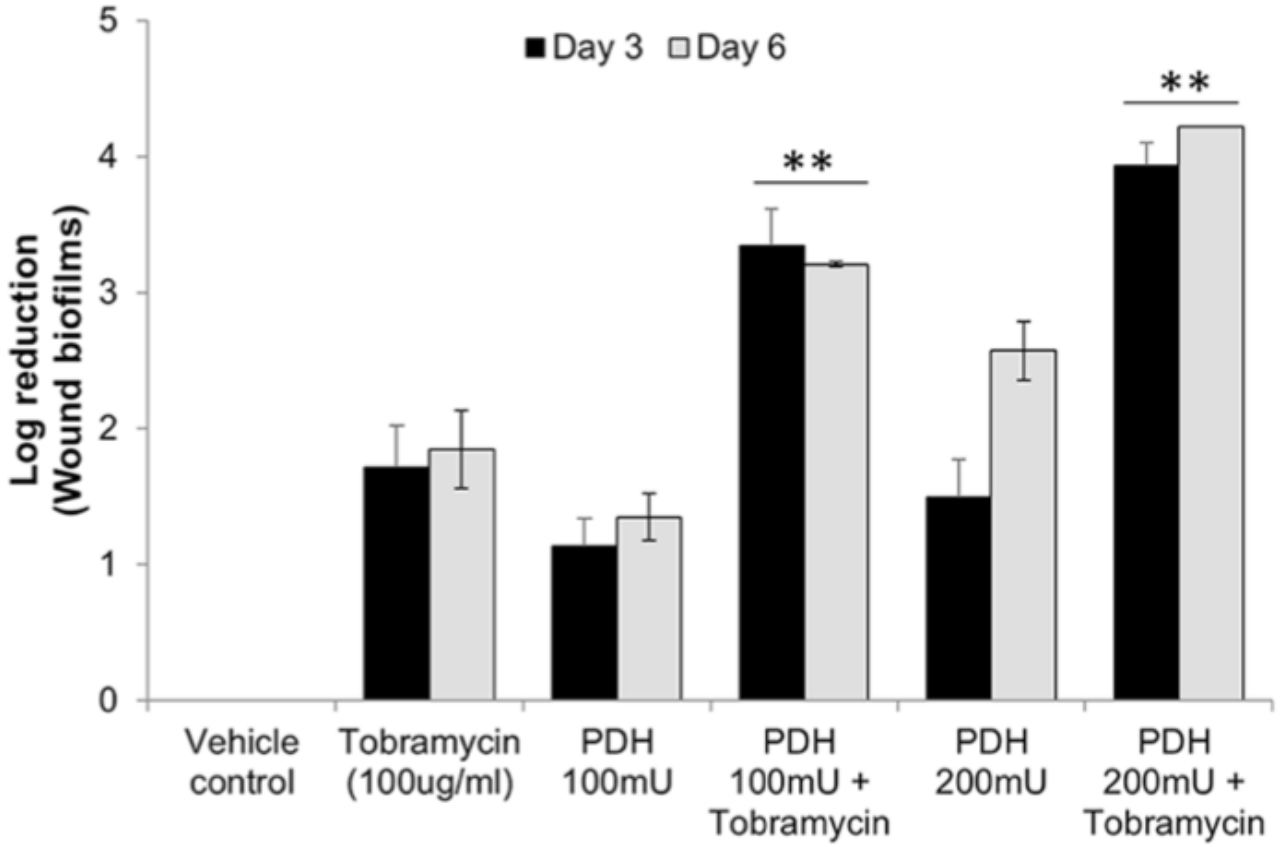

Figure 1. Efficacy of PDH (100 and 200 mU), tobramycin (100 μg/ ml), or co-treatment of PDH and tobramycin on the P. aeruginosa biofilm population.[12] Each experiment was done in triplicate, with each biological replicate being comprised of 3 wounds per treatment group (n = 9). Error bars represent standard deviation. **Significantly different ($p < 0.05$) from wounds treated only with PDH or tobramycin.

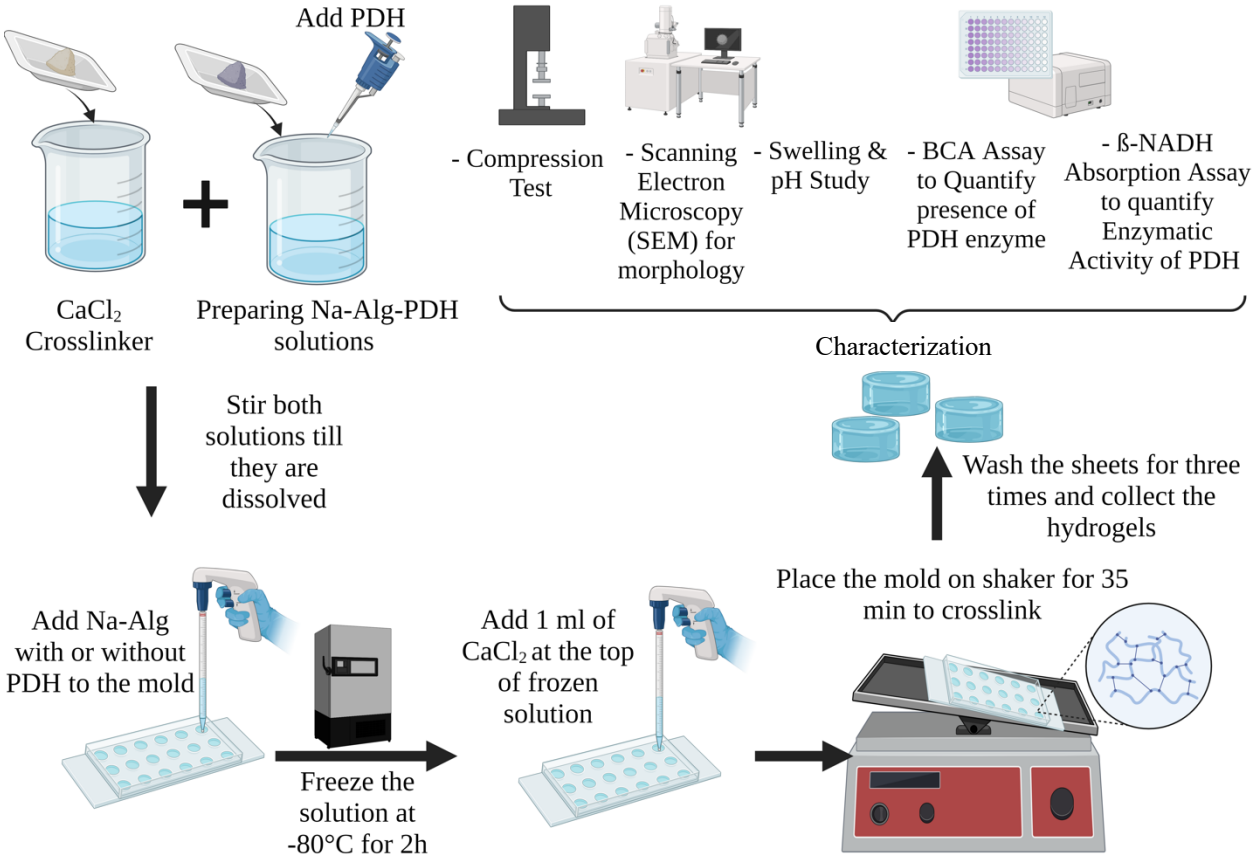

Figure 2. Synthesis of alginate-PDH sheets with and without PDH to be used in downstream testing such as compression testing, scanning electron microscopy, swelling and pH studies, BCA assays, and β-NADH absorption assay. Created on BioRender by Omid Sedighi.

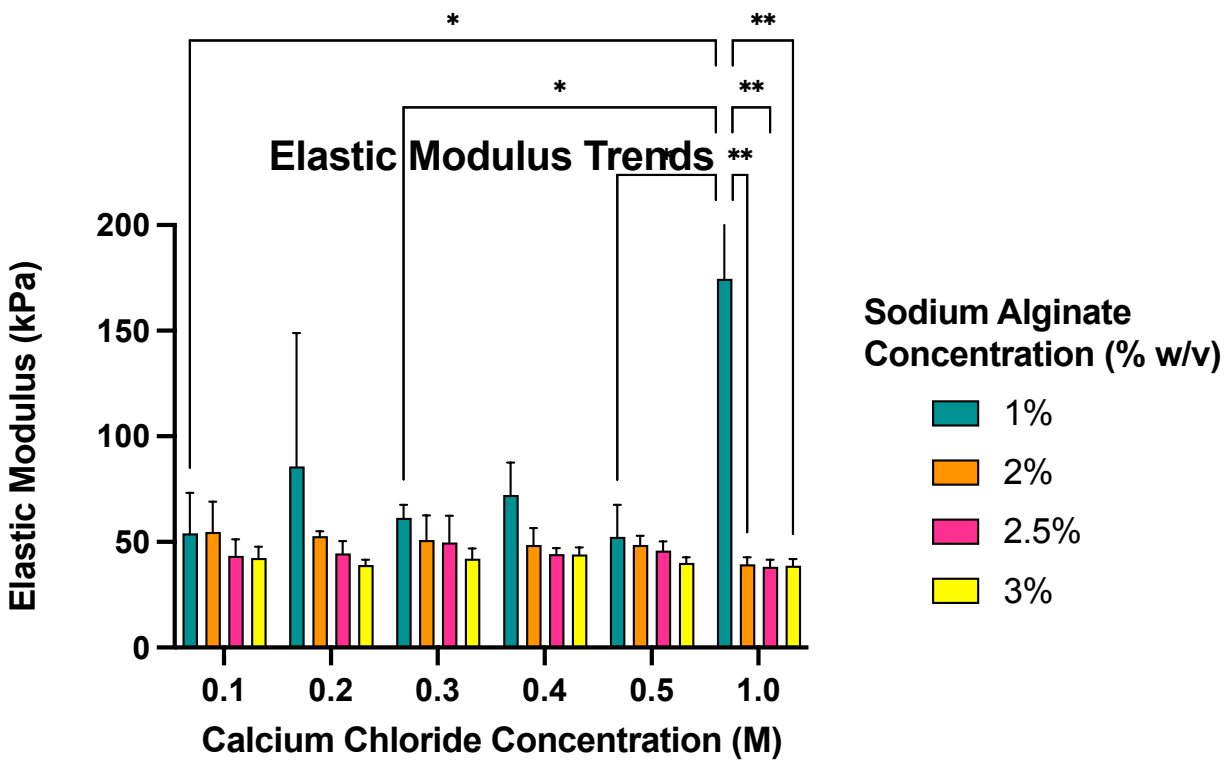

Figure 3. Elastic modulus results from each hydrogel formulation (n = 4). The elastic modulus appears to decrease as sodium alginate concentration increases but is not significant ($\alpha = 0.05$) within each calcium chloride concentration. Error bars represent standard deviation.

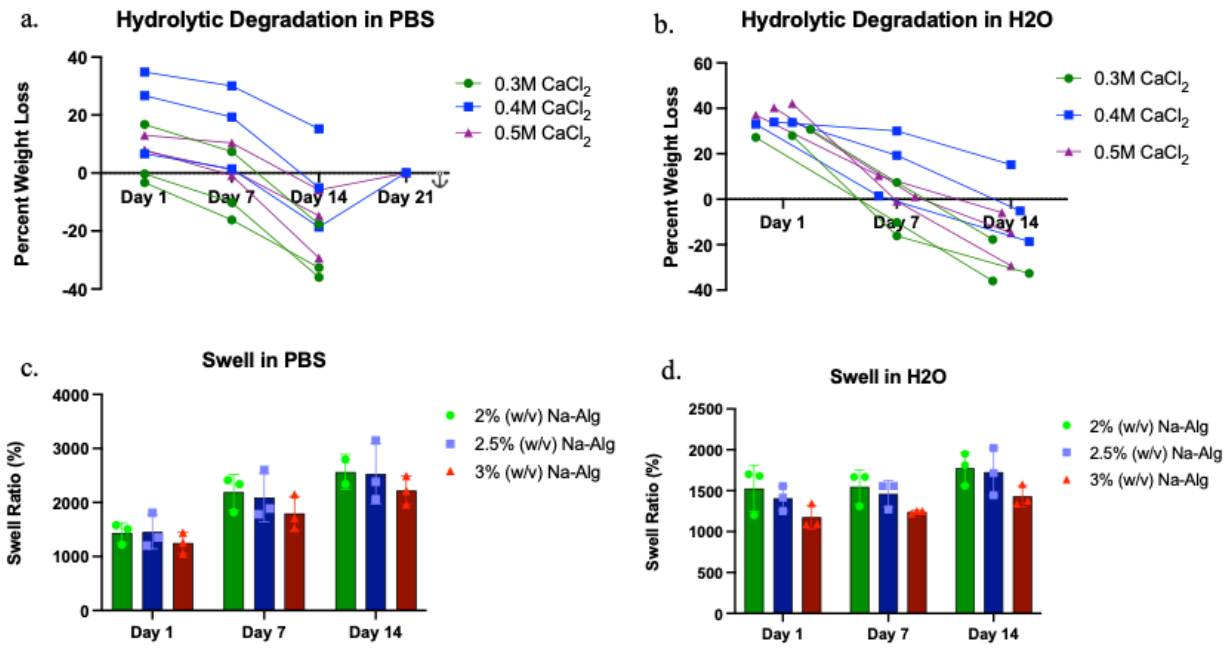

Figure 4. Hydrolytic degradation in a) PBS and b) water to determine the effect of salts on percent weight loss. Sheets generally degraded the most within the first 7 days. Swell ratio in a) PBS and b) water. There is a sodium alginate concentration dependent trend in swell ratio, where higher concentrations produce lower swell ratios. Error bars represent standard deviation.

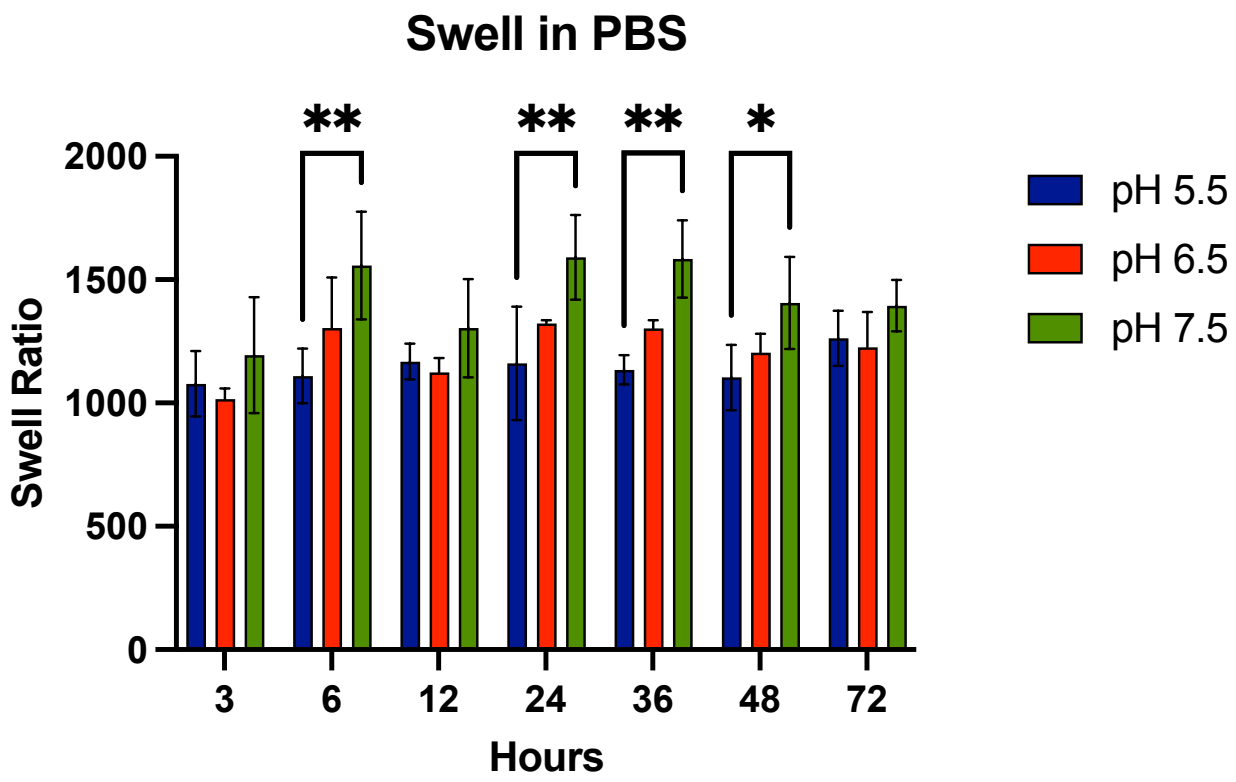

Figure 5. Swell ratio results in varying pH PBS solutions over 72 hours. There appears to be a positive trend with swell ratio and increase in pH. There is a significant difference in swell ratio between pH 5.5 and 7.5 at hours 6 ($p = 0.0013$), 24 ($p = 0.0021$), 36 ($p = 0.0013$), and 48 ($p = 0.0368$). Error bars represent standard deviation.

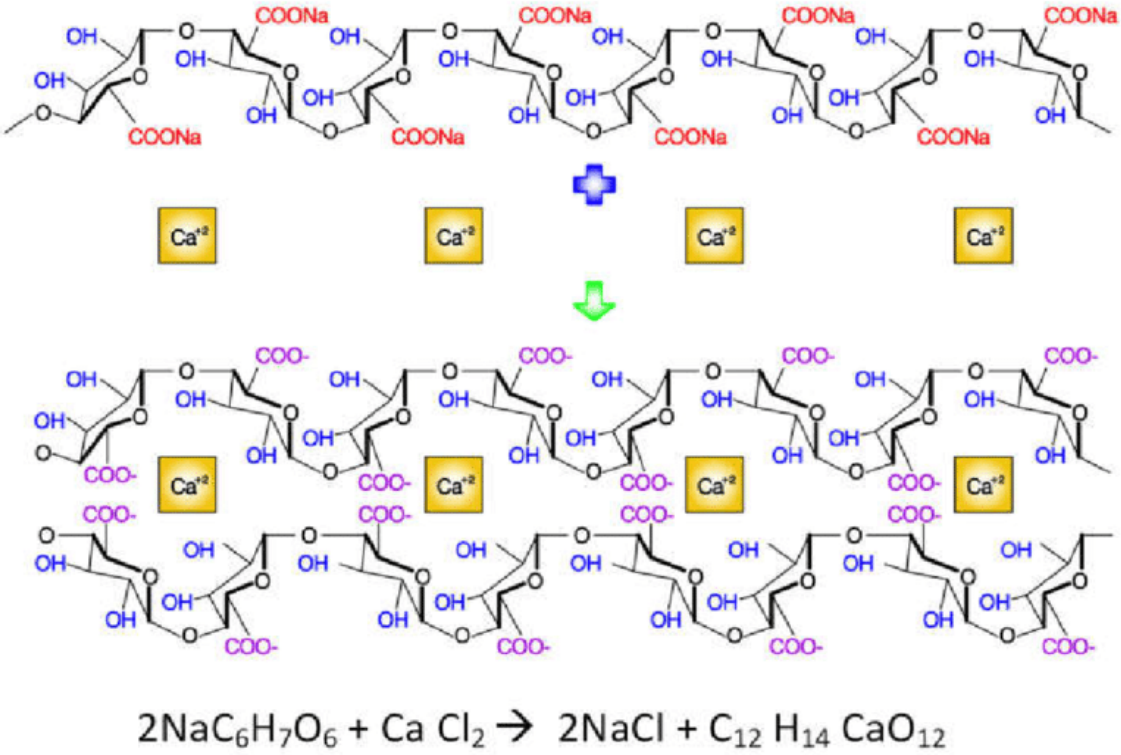

$$2NaC_6H_7O_6 + Ca\ Cl_2 \rightarrow 2NaCl + C_{12}\ H_{14}\ CaO_{12}$$

Figure 6. A depiction of ionic crosslinking of sodium alginate and calcium chloride.32 Calcium ions ionically bond with carboxyl groups of alginate backbone to form an egg crate structure.

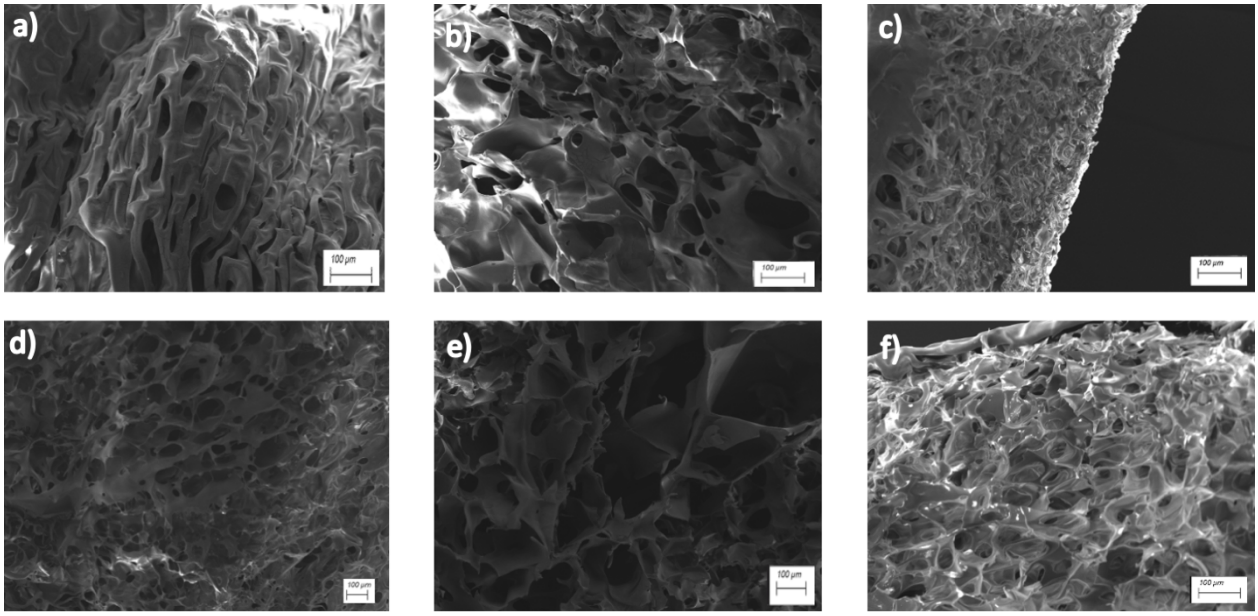

Figure 7. SEM results displaying pore size of hydrogels (scale bar = 100 μm). The top row are images of the external surface of the hydrogel sheets: a) 2% Na-Alg & 0.3 M $CaCl_2$, b) 2% Na-Alg & 0.5 M $CaCl_2$, c) 3% Na-Alg & 0.5 M $CaCl_2$. The bottom row are images of the cross-sectional surface of hydrogel sheets after being cut with a razorblade: d) 2% Na-Alg & 0.3 M $CaCl_2$, e) 2% Na-Alg & 0.5 M $CaCl_2$, f) 3% Na-Alg & 0.5 M $CaCl_2$.

Table 1.

Hydrogel concentration matrix of samples produced for initial compression testing (n = 4 of each formulation). Highlighted concentrations were used for preliminary swell ratio and hydrolytic degradation studies.

Sodium Alginate	**Calcium Chloride Concentration (M)**					
Concentration (% w/v)	**0.1**	**0.2**	**0.3**	**0.4**	**0.5**	**1.0**
1						
2						
2.5						
3						

Table 2.

SEM results on 3 compositions of hydrogel sheets. Pore sizes ranged from 12.5 – 194.2 µm.

Formulation	**External Surface (µm): Mean ± SD**	**Cross-Sectional Surface (µm): Mean ± SD**
2% Na-Alg & 0.3 M $CaCl_2$	45.409 ± 28.906 (n = 20)	88.375 ± 39.329 (n = 29)
2.5% Na-Alg & 0.5 M $CaCl_2$	40.607 ± 32.555 (n = 14)	60.969 ± 24.455 (n = 10)
3% Na-Alg & 0.5 M $CaCl_2$	25.726 ± 16.969 (n = 3)	43.853 ± 23.954 (n = 11)

Table 3.

Activity and protein concentration from pyruvate assay and BCA assays. Values are expressed as mean ± standard deviation (n = 3). In the Free PDH samples, activity levels off after 90 minutes. In the hydrogel sheets, activity and PDH concentration increases in a concentration dependent manner. Activity levels off after 1080 minutes in hydrogel sheets.

ID	**Amount of PDH loaded (mU)**	**Enzyme Activity (mU/mL)**				**PDH Concentration (mg/mL)**
		T = 0	*T = 60 min*	*T = 90 min*	*T = 1080 min*	
Free PDH	330	-	9.766 ± 0.226	8.058 ± 0.260	-	-
Encapsulated	0	-	0	0	0	-
Encapsulated	2084	-	0.536 ± 0.180	0.711 ± 0.073	0.289 ± 0.017	43.162
Encapsulated	2778	-	1.297 ± 0.694	1.569 ± 0.539	0.403 ± 0.188	43.628
Encapsulated	3473	-	1.930 ± 0.128	2.026 ± 0.168	0.552 ± 0.075	47.140

References

(1) Flemming, H.-C.; Wingender, J.; Szewzyk, U.; Steinberg, P.; Rice, S. A.; Kjelleberg, S. Biofilms: an emergent form of bacterial life. *Nature Reviews Microbiology* **2016**, *14* (9), 563-575. DOI: 10.1038/nrmicro.2016.94.

(2) Kennedy, P.; Brammah, S.; Wills, E. Burns, biofilm and a new appraisal of burn wound sepsis. *Burns* **2010**, *36* (1), 49-56. DOI: 10.1016/j.burns.2009.02.017 From NLM.

(3) Rezvani Ghomi, E.; Khalili, S.; Nouri Khorasani, S.; Esmaeely Neisiany, R.; Ramakrishna, S. Wound dressings: Current advances and future directions. *Journal of Applied Polymer Science* **2019**, *136* (27), 47738. DOI: https://doi.org/10.1002/app.47738.

(4) Powers, J. G.; Morton, L. M.; Phillips, T. J. Dressings for chronic wounds. *Dermatol Ther* **2013**, *26* (3), 197-206. DOI: 10.1111/dth.12055 From NLM.

(5) Rather, M. A.; Gupta, K.; Bardhan, P.; Borah, M.; Sarkar, A.; Eldiehy, K. S. H.; Bhuyan, S.; Mandal, M. Microbial biofilm: A matter of grave concern for human health and food industry. *J Basic Microbiol* **2021**, *61* (5), 380-395. DOI: 10.1002/jobm.202000678 From NLM.

(6) Wolcott, R. D.; Rhoads, D. D.; Bennett, M. E.; Wolcott, B. M.; Gogokhia, L.; Costerton, J. W.; Dowd, S. E. Chronic wounds and the medical biofilm paradigm. *J Wound Care* **2010**, *19* (2), 45-46, 48-50, 52-43. DOI: 10.12968/jowc.2010.19.2.46966 From NLM.

(7) Sen, C. K.; Gordillo, G. M.; Roy, S.; Kirsner, R.; Lambert, L.; Hunt, T. K.; Gottrup, F.; Gurtner, G. C.; Longaker, M. T. Human skin wounds: a major and snowballing threat to public health and the economy. *Wound Repair Regen* **2009**, *17* (6), 763-771. DOI: 10.1111/j.1524-475X.2009.00543.x From NLM.

(8) Church, D.; Elsayed, S.; Reid, O.; Winston, B.; Lindsay, R. Burn wound infections. *Clin Microbiol Rev* **2006**, *19* (2), 403-434. DOI: 10.1128/cmr.19.2.403-434.2006 From NLM.

(9) McManus, W. F.; Goodwin, C. W.; Mason, A. D., Jr.; Pruitt, B. A., Jr. Burn wound infection. *J Trauma* **1981**, *21* (9), 753-756. DOI: 10.1097/00005373-198109000-00001 From NLM.

(10) Cardona, A. F.; Wilson, S. E. Skin and soft-tissue infections: a critical review and the role of telavancin in their treatment. *Clin Infect Dis* **2015**, *61 Suppl 2*, S69-78. DOI: 10.1093/cid/civ528 From NLM.

(11) Negut, I.; Grumezescu, V.; Grumezescu, A. M. Treatment Strategies for Infected Wounds. *Molecules* **2018**, *23* (9). DOI: 10.3390/molecules23092392 From NLM.

(12) Goodwine, J.; Gil, J.; Doiron, A.; Valdes, J.; Solis, M.; Higa, A.; Davis, S.; Sauer, K. Pyruvate-depleting conditions induce biofilm dispersion and enhance the efficacy of antibiotics in killing biofilms in vitro and in vivo. *Scientific Reports* **2019**, *9* (1), 3763. DOI: 10.1038/s41598-019-40378-z.

(13) Mah, T. F.; O'Toole, G. A. Mechanisms of biofilm resistance to antimicrobial agents. *Trends Microbiol* **2001**, *9* (1), 34-39. DOI: 10.1016/s0966-842x(00)01913-2 From NLM.

(14) Nickel, J. C.; Ruseska, I.; Wright, J. B.; Costerton, J. W. Tobramycin resistance of Pseudomonas aeruginosa cells growing as a biofilm on urinary catheter material. *Antimicrobial Agents and Chemotherapy* **1985**, *27* (4), 619-624. DOI: doi:10.1128/aac.27.4.619.

(15) Davies, D. Understanding biofilm resistance to antibacterial agents. *Nat Rev Drug Discov* **2003**, *2* (2), 114-122. DOI: 10.1038/nrd1008 From NLM.

(16) Teitzel, G. M.; Parsek, M. R. Heavy metal resistance of biofilm and planktonic Pseudomonas aeruginosa. *Appl Environ Microbiol* **2003**, *69* (4), 2313-2320. DOI: 10.1128/aem.69.4.2313-2320.2003 From NLM.

(17) Welin-Neilands, J.; Svensäter, G. Acid tolerance of biofilm cells of Streptococcus mutans. *Appl Environ Microbiol* **2007**, *73* (17), 5633-5638. DOI: 10.1128/aem.01049-07 From NLM.

(18) Hall-Stoodley, L.; Costerton, J. W.; Stoodley, P. Bacterial biofilms: from the natural environment to infectious diseases. *Nat Rev Microbiol* **2004**, *2* (2), 95-108. DOI: 10.1038/nrmicro821 From NLM.

(19) Espeland, E. M.; Wetzel, R. G. Complexation, Stabilization, and UV Photolysis of Extracellular and Surface-Bound Glucosidase and Alkaline Phosphatase: Implications for Biofilm Microbiota. *Microb Ecol* **2001**, *42* (4), 572-585. DOI: 10.1007/s00248-001-1023-7 From NLM.

(20) Schaudinn, C.; Stoodley, P.; Kainović, A.; O'Keefe, T.; Costerton, J.; Robinson, D.; Baum, M.; Erhlich, G.; Webster, P. Bacterial Biofilms, Other Structures Seen as Mainstream Concepts. *Microbe* **2006**, *2*, 231-237. DOI: 10.1128/microbe.2.231.1.

(21) Donlan, R. M. Biofilms and device-associated infections. *Emerg Infect Dis* **2001**, *7* (2), 277-281. DOI: 10.3201/eid0702.010226 From NLM.

(22) Costerton, J. W. Biofilm theory can guide the treatment of device-related orthopaedic infections. *Clin Orthop Relat Res* **2005**, (437), 7-11. DOI: 10.1097/00003086-200508000-00003 From NLM.

(23) Wilson, M. Bacterial biofilms and human disease. *Sci Prog* **2001**, *84* (Pt 3), 235-254. DOI: 10.3184/003685001783238998 From NLM.

(24) Funari, R.; Shen, A. Q. Detection and Characterization of Bacterial Biofilms and Biofilm-Based Sensors. *ACS Sensors* **2022**, *7* (2), 347-357. DOI: 10.1021/acssensors.1c02722.

(25) Petrova, O. E.; Sauer, K. Escaping the biofilm in more than one way: desorption, detachment or dispersion. *Curr Opin Microbiol* **2016**, *30*, 67-78. DOI: 10.1016/j.mib.2016.01.004 From NLM.

(26) Gupta, K.; Marques Cláudia, N. H.; Petrova Olga, E.; Sauer, K. Antimicrobial Tolerance of Pseudomonas aeruginosa Biofilms Is Activated during an Early Developmental Stage and Requires the Two-Component Hybrid SagS. *Journal of Bacteriology* **2013**, *195* (21), 4975-4987. DOI: 10.1128/jb.00732-13 (acccessed 2024/04/22).

(27) Han, C.; Goodwine, J.; Romero, N.; Steck, K. S.; Sauer, K.; Doiron, A. Enzyme-encapsulating polymeric nanoparticles: A potential adjunctive therapy in Pseudomonas aeruginosa biofilm-associated infection treatment. *Colloids Surf B Biointerfaces* **2019**, *184*, 110512. DOI: 10.1016/j.colsurfb.2019.110512 From NLM.

(28) Atiyeh, B. S.; Costagliola, M.; Hayek, S. N.; Dibo, S. A. Effect of silver on burn wound infection control and healing: Review of the literature. *Burns* **2007**, *33* (2), 139-148. DOI: https://doi.org/10.1016/j.burns.2006.06.010.

(29) Lansdown, A. B. Silver. I: Its antibacterial properties and mechanism of action. *J Wound Care* **2002**, *11* (4), 125-130. DOI: 10.12968/jowc.2002.11.4.26389 From NLM.

(30) Zaman, H. U.; Islam, J. M. M.; Khan, M. A.; Khan, R. A. Physico-mechanical properties of wound dressing material and its biomedical application. *Journal of the Mechanical Behavior of Biomedical Materials* **2011**, *4* (7), 1369-1375. DOI: https://doi.org/10.1016/j.jmbbm.2011.05.007.

(31) Özcan Bülbül, E.; Okur, M. E.; Üstündağ Okur, N.; Siafaka, P. I. Chapter 2 - Traditional and advanced wound dressings: physical characterization and desirable properties for wound healing. In *Natural Polymers in Wound Healing and Repair*, Sah, M. K., Kasoju, N., Mano, J. F. Eds.; Elsevier, 2022; pp 19-50.

(32) Lu, H.; Butler, J.; Britten, N.; Venkatraman, P.; Rahatekar, S. Natural Antimicrobial Nano Composite Fibres Manufactured from a Combination of Alginate and Oregano Essential Oil. *Nanomaterials* **2021**, *11*, 2062. DOI: 10.3390/nano11082062.

(33) Berger, J.; Reist, M.; Mayer, J. M.; Felt, O.; Peppas, N. A.; Gurny, R. Structure and interactions in covalently and ionically crosslinked chitosan hydrogels for biomedical applications. *Eur J Pharm Biopharm* **2004**, *57* (1), 19-34. DOI: 10.1016/s0939-6411(03)00161-9 From NLM.

(34) Aderibigbe, B. A.; Buyana, B. Alginate in Wound Dressings. *Pharmaceutics* **2018**, *10* (2). DOI: 10.3390/pharmaceutics10020042 From NLM.

(35) Pereira, R. F.; Carvalho, A.; Gil, M. H.; Mendes, A.; Bártolo, P. J. Influence of Aloe vera on water absorption and enzymatic in vitro degradation of alginate hydrogel films. *Carbohydrate Polymers* **2013**, *98* (1), 311-320. DOI: https://doi.org/10.1016/j.carbpol.2013.05.076.

(36) Dodero, A.; Alberti, S.; Gaggero, G.; Ferretti, M.; Botter, R.; Vicini, S.; Castellano, M. An Up-to-Date Review on Alginate Nanoparticles and Nanofibers for Biomedical and Pharmaceutical Applications. *Advanced Materials Interfaces* **2021**, *8* (22), 2100809. DOI: https://doi.org/10.1002/admi.202100809.

(37) Guziewicz, N.; Best, A.; Perez-Ramirez, B.; Kaplan, D. L. Lyophilized silk fibroin hydrogels for the sustained local delivery of therapeutic monoclonal antibodies. *Biomaterials* **2011**, *32* (10), 2642-2650. DOI: https://doi.org/10.1016/j.biomaterials.2010.12.023.

(38) Petrova, O. E.; Schurr, J. R.; Schurr, M. J.; Sauer, K. Microcolony formation by the opportunistic pathogen Pseudomonas aeruginosa requires pyruvate and pyruvate fermentation. *Molecular Microbiology* **2012**, *86* (4), 819-835. DOI: https://doi.org/10.1111/mmi.12018.

(39) Filkins, L. M.; O'Toole, G. A. Cystic Fibrosis Lung Infections: Polymicrobial, Complex, and Hard to Treat. *PLOS Pathogens* **2016**, *11* (12), e1005258. DOI: 10.1371/journal.ppat.1005258.

(40) Gray, L. R.; Tompkins, S. C.; Taylor, E. B. Regulation of pyruvate metabolism and human disease. *Cell Mol Life Sci* **2014**, *71* (14), 2577-2604. DOI: 10.1007/s00018-013-1539-2 From NLM.

(41) Grewal, S. W. M. *Fermentation*.

CK-12, 2018.

https://bio.libretexts.org/Courses/Community_College_of_Vermont/Human_Biology_(Gabor_Gyurkovics)/03%3A_Cells/3.10%3A_Fermentation (accessed 2/8/2024).

(42) Westin, J. *Fermentation (anaerobic glycolysis)*. https://jackwestin.com/resources/mcat-content/glycolysis-gluconeogenesis-and-the-pentose-phosphate-pathway/fermentation-anaerobic-glycolysis (accessed 2/8/2024).

(43) Reyhanoglu, G.; Reddivari, A. K. R. Tobramycin. In *StatPearls*, StatPearls Publishing Copyright © 2024, StatPearls Publishing LLC., 2024.

(44) Shorrock, S. M. The Exploration of Tissue pH and its Relationship to Bacterial Contamination. Worcester Polytechnic Institute, 2000. https://digital.wpi.edu/show/2f75r8056 https://digital.wpi.edu/show/4b29b604b.

(45) Schneider, L. A.; Korber, A.; Grabbe, S.; Dissemond, J. Influence of pH on wound-healing: a new perspective for wound-therapy? *Arch Dermatol Res* **2007**, *298* (9), 413-420. DOI: 10.1007/s00403-006-0713-x From NLM.

(46) Sumegi, B.; Liposits, Z.; Inman, L.; Paull, W. K.; Srere, P. A. Electron microscopic study on the size of pyruvate dehydrogenase complex in situ. *Eur J Biochem* **1987**, *169* (1), 223-230. DOI: 10.1111/j.1432-1033.1987.tb13601.x From NLM.

(47) Chan, A. W.; Neufeld, R. J. Modeling the controllable pH-responsive swelling and pore size of networked alginate based biomaterials. *Biomaterials* **2009**, *30* (30), 6119-6129. DOI: 10.1016/j.biomaterials.2009.07.034 From NLM.

(48) Tahir, I.; Floreani, R. Dual-Crosslinked Alginate-Based Hydrogels with Tunable Mechanical Properties for Cultured Meat. *Foods* **2022**, *11* (18), 2829.

(49) Jeon, O.; Bouhadir, K. H.; Mansour, J. M.; Alsberg, E. Photocrosslinked alginate hydrogels with tunable biodegradation rates and mechanical properties. *Biomaterials* **2009**, *30* (14), 2724-2734. DOI: https://doi.org/10.1016/j.biomaterials.2009.01.034.

(50) Saarai, A.; Sedlacek, T.; Kasparkova, V.; Kitano, T.; Saha, P. On the characterization of sodium alginate/gelatine-based hydrogels for wound dressing. *Journal of Applied Polymer Science* **2012**, *126* (S1), E79-E88. DOI: https://doi.org/10.1002/app.36590.

(51) Bettadapur, A.; Suh, G. C.; Geisse, N. A.; Wang, E. R.; Hua, C.; Huber, H. A.; Viscio, A. A.; Kim, J. Y.; Strickland, J. B.; McCain, M. L. Prolonged Culture of Aligned Skeletal Myotubes on Micromolded Gelatin Hydrogels. *Scientific Reports* **2016**, *6* (1), 28855. DOI: 10.1038/srep28855.

(52) He, X.; Liu, Y.; Li, H.; Li, H. Single-stranded structure of alginate and its conformation evolvement after an interaction with calcium ions as revealed by electron microscopy. *RSC Advances* **2016**, *6* (115), 114779-114782, 10.1039/C6RA22212A. DOI: 10.1039/C6RA22212A.

(53) Grant, G. T.; Morris, E. R.; Rees, D. A.; Smith, P. J. C.; Thom, D. Biological interactions between polysaccharides and divalent cations: The egg-box model. *FEBS Letters* **1973**, *32* (1), 195-198. DOI: https://doi.org/10.1016/0014-5793(73)80770-7.

(54) Kaklamani, G.; Cheneler, D.; Grover, L. M.; Adams, M. J.; Bowen, J. Mechanical properties of alginate hydrogels manufactured using external gelation. *Journal of the Mechanical Behavior of Biomedical Materials* **2014**, *36*, 135-142. DOI: https://doi.org/10.1016/j.jmbbm.2014.04.013.

(55) Mokhena, T. C.; Mochane, M. J.; Mtibe, A.; John, M. J.; Sadiku, E. R.; Sefadi, J. S. Electrospun Alginate Nanofibers Toward Various Applications: A Review. *Materials (Basel)* **2020**, *13* (4). DOI: 10.3390/ma13040934 From NLM.

(56) Xue, J.; Wu, T.; Dai, Y.; Xia, Y. Electrospinning and Electrospun Nanofibers: Methods, Materials, and Applications. *Chem Rev* **2019**, *119* (8), 5298-5415. DOI: 10.1021/acs.chemrev.8b00593 From NLM.

(57) Banerjee, A.; Arha, M.; Choudhary, S.; Ashton, R. S.; Bhatia, S. R.; Schaffer, D. V.; Kane, R. S. The influence of hydrogel modulus on the proliferation and differentiation of encapsulated neural stem cells. *Biomaterials* **2009**, *30* (27), 4695-4699. DOI: 10.1016/j.biomaterials.2009.05.050 From NLM.

(58) Peng, C.-W.; Lin, H.-Y.; Wang, H.-W.; Wu, W.-W. The influence of operating parameters on the drug release and anti-bacterial performances of alginate wound dressings prepared by three-dimensional plotting. *Materials Science and Engineering: C* **2012**, *32* (8), 2491-2500. DOI: https://doi.org/10.1016/j.msec.2012.07.031.

(59) Budianto, E.; Muthoharoh, S. P.; Nizardo, N. M. Effect of crosslinking agents, pH and temperature on swelling behavior of cross-linked chitosan hydrogel. *Asian Journal of Applied Sciences* **2015**, *3* (5).

(60) Subramani, R.; Izquierdo-Alvarez, A.; Bhattacharya, P.; Meerts, M.; Moldenaers, P.; Ramon, H.; Van Oosterwyck, H. The Influence of Swelling on Elastic Properties of Polyacrylamide Hydrogels. *Frontiers in Materials* **2020**, *7*, Original Research. DOI: 10.3389/fmats.2020.00212.

(61) Kimmel, H. M.; Grant, A.; Ditata, J. The Presence of Oxygen in Wound Healing. *Wounds* **2016**, *28* (8), 264-270. From NLM.

(62) Wang, C.-H.; Hsieh, D.-J.; Periasamy, S.; Chuang, C.-T.; Tseng, F.-W.; Kuo, J.-C.; Tarng, Y.-W. Regenerative porcine dermal collagen matrix developed by supercritical carbon dioxide extraction technology: Role in accelerated wound healing. *Materialia* **2020**, *9*, 100576. DOI: https://doi.org/10.1016/j.mtla.2019.100576.

(63) Tegl, G.; Schiffer, D.; Sigl, E.; Heinzle, A.; Guebitz, G. M. Biomarkers for infection: enzymes, microbes, and metabolites. *Appl Microbiol Biotechnol* **2015**, *99* (11), 4595-4614. DOI: 10.1007/s00253-015-6637-7 From NLM.

(64) Sutendra, G.; Kinnaird, A.; Dromparis, P.; Paulin, R.; Stenson, Trevor H.; Haromy, A.; Hashimoto, K.; Zhang, N.; Flaim, E.; Michelakis, Evangelos D. A Nuclear Pyruvate Dehydrogenase Complex Is Important for the Generation of Acetyl-CoA and Histone Acetylation. *Cell* **2014**, *158* (1), 84-97. DOI: 10.1016/j.cell.2014.04.046 (acccessed 2024/03/28).

(65) Gu, Y.; Zhou, Z. H.; McCarthy, D. B.; Reed, L. J.; Stoops, J. K. 3D electron microscopy reveals the variable deposition and protein dynamics of the peripheral pyruvate dehydrogenase component about the core. *Proceedings of the National Academy of Sciences* **2003**, *100* (12), 7015-7020. DOI: doi:10.1073/pnas.0732060100.

(66) Zhu, A.; Romero, R.; Petty, H. R. A sensitive fluorimetric assay for pyruvate. *Anal Biochem* **2010**, *396* (1), 146-151. DOI: 10.1016/j.ab.2009.09.017 From NLM.

(67) Williams, M.; Randall, D. D. Pyruvate Dehydrogenase Complex from Chloroplasts of Pisum sativum L. *Plant Physiol* **1979**, *64* (6), 1099-1103. DOI: 10.1104/pp.64.6.1099 From NLM.